energy&fuels

Article

Cite This: Energy Fuels 2018, 32, 11970−11978

pubs.acs.org/EF

Kinetic Effects of *n*-Heptane Addition on Low and High Temperature Oxidation of Methane in a Jet-Stirred Reactor

Zunhua Zhang,[†,‡,§,#] Hao Zhao,[*,§,#] Ling Cao,[†,‡] Gesheng Li,[†,‡] and Yiguang Ju[§]

[†]Key Laboratory of High Performance Ship Technology Wuhan University of Technology, Ministry of Education, Wuhan, Hubei 430063, P. R. China

[‡]School of Energy and Power Engineering, Wuhan University of Technology, Wuhan, Hubei 430063, P. R. China

[§]Department of Mechanical and Aerospace Engineering, Princeton University, Princeton, New Jersey 08544-5263, United States

ABSTRACT: The kinetic effects of *n*-heptane addition on low and high temperature oxidations of methane were experimentally investigated over a range of temperatures from 800 to 1200 K, at the equivalence ratio of 0.5 in an atmospheric jet-stirred reactor (JSR). The *n*-heptane content in the methane/*n*-heptane mixture was varied between 0 and 100%. The mole fractions of CH_4, nC_7H_{16}, O_2, CO, CO_2, CH_2O, and C_2H_4 were determined respectively in the present experiments, and the NUI mechanism was employed to perform the numerical studies under the same conditions by using the perfectly stirred reactor model. The results show that the onset temperature of the oxidation of methane decreases with the increase of the *n*-heptane content in methane/*n*-heptane mixture significantly, and that even a small amount of *n*-heptane can cause an obvious shift of high temperature oxidation of methane to lower temperature. According to the reaction path analysis, the initial kinetic enhancement reactions of *n*-heptane in the oxidation of methane are identified. It is shown that the kinetic enhancement of methane oxidation by *n*-heptane addition increases at low temperature. The sensitivity analysis of the mole fraction of methane indicate that the methane oxidation is mainly sensitive to those relevant reactions involving OH, HO_2, and other radicals produced by *n*-heptane at low temperature, and especially at low *n*-heptane content through the radical pool enrichment. The present study indicates the potential of *n*-heptane-assisted methane combustion in diesel and marine engine applications.

1. INTRODUCTION

Natural gas has been emerging as a promising alternative fuel recently, due to its economic and environmental advantages compared to gasoline and diesel. Because of the high ratio of hydrogen to carbon, natural gas is expected to significantly reduce the carbon dioxide emissions.[1,2] Meanwhile, natural gas has a higher octane number than conventional fossil fuels, which means that a larger compression ratio and higher thermal efficiency can be achieved in the engines fueled with natural gas.[3,4] Unfortunately, due to the slow reactivity of methane at low temperature, it is quite difficult to ignite natural gas through compression in compression ignition (CI) engines. To overcome the problem, the natural gas−diesel dual-fuel engine was developed.[5−8] In the dual-fuel engines, natural gas is ignited by a small amount of diesel and its ignition and combustion processes may be affected by the pilot diesel, which has a direct impact on the ignition performance and emission behaviors of the engines.[9−12] Therefore, it is important to study the kinetic effects of diesel addition to natural gas for the better design and optimization of the dual-fuel engines.

Natural gas and diesel are both complex mixtures composed of many different species, which makes it difficult to perform the kinetic studies for the real fuel mixtures. Consequently, surrogate fuel models are proposed to make it possible to study the chemical kinetics of the complex mixtures.[13−16] As the main component of natural gas, methane is always used as the representative of natural gas,[17,18] while *n*-heptane is considered as a single surrogate of diesel because of their similar cetane numbers and low temperature ignition behavior.[19−22] Thus, in the present study, the methane/*n*-heptane mixture is selected as the surrogate model of natural gas−diesel dual-fuel to understand the kinetic coupling between natural gas and diesel at low and high temperature.

Methane is a relatively stable species due to high carbon−hydrogen bond energy in the methane molecule structure,[23−25] whereas *n*-heptane shows high reactivity at low temperature through the low temperature chemistry pathway.[26,27] The different reactivities between methane and *n*-heptane and the strong nonlinearity of the chemical reaction process lead to an increased difficulty in relevant studies,[23−25,28−30] and as a result, only little information about the kinetic effects of *n*-heptane addition to methane is available from the open literature. Aggarwal et al.[31] numerically studied the ignition characteristics of the methane/*n*-heptane mixture, and found that the ignition delay time of the methane/*n*-heptane mixture can be obviously reduced by *n*-heptane, implying that the ignition behavior of the mixture was primarily dominated by the oxidation chemistry of *n*-heptane. Wang et al.[32] also carried out computations of the flame development in *n*-heptane/methane−air mixing layers under various conditions. The characteristic time required for steady flame propagation was investigated and its dependence on pressure, initial CH_4/air temperature, premixed equivalence ratio, and initial mixing layer thickness had been examined. Li et al.[33] performed an experimental investigation on laminar burning velocities and Markstein lengths of premixed methane−*n*-heptane−air mixtures in a combustion chamber, and the

Received: September 5, 2018
Revised: October 25, 2018
Published: October 29, 2018

DOI: 10.1021/acs.energyfuels.8b03124
Energy Fuels 2018, 32, 11970−11978

Table 1. Experimental Conditions

mixture	CH_4 (%)	nC_7H_{16} (%)	O_2 (%)	Ar (%)	N_2 (%)	flow rate (mL/min)	temp range (K)
M0	1.0	0.0	4.0	2.0	93.0	1800	1000−1200
M10	0.9	0.1	5.8	2.0	91.2	1800	800−1100
M50	0.5	0.5	13.0	2.0	84.0	1800	800−1100
M100	0.0	0.5	11.0	2.0	86.5	1800	800−1100

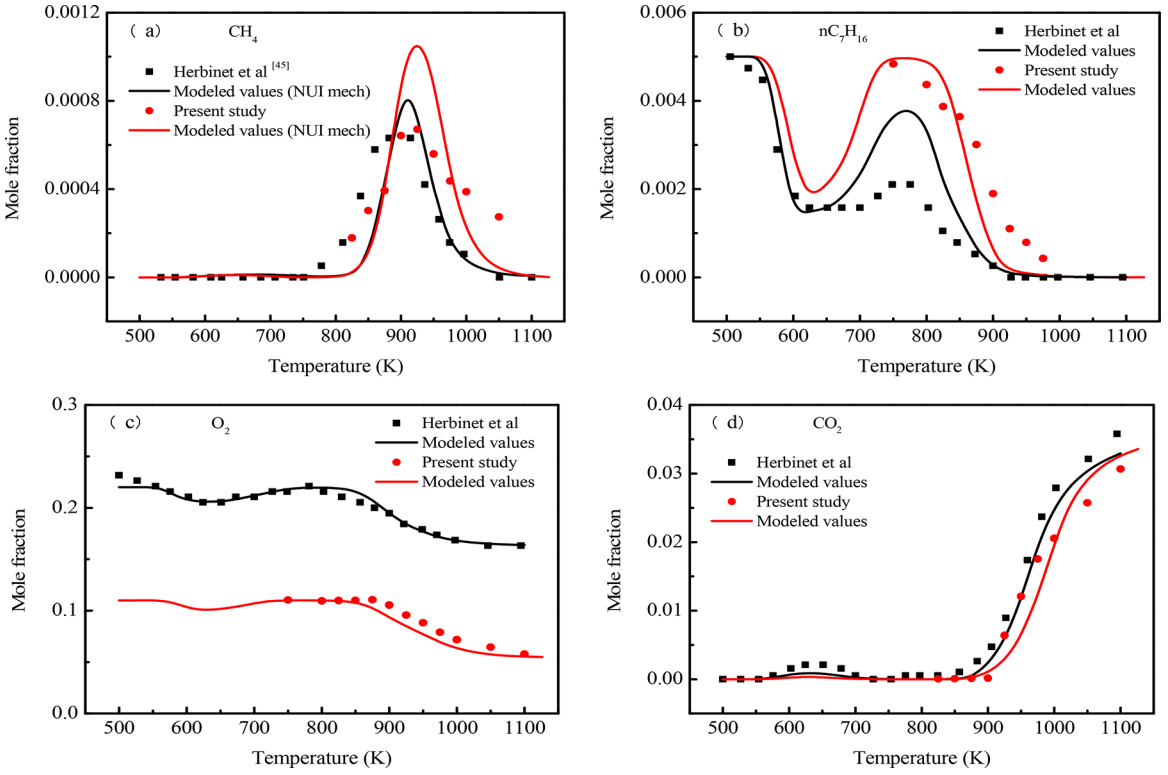

Figure 1. Comparisons of the mole fractions of major species in the oxidation of *n*-heptane between the present (ϕ = 0.5, P = 1 atm, 0.5%nC_7H_{16}−11%O_2−2%Ar-86.5%N_2) and other study (ϕ = 0.25, P = 1 atm, 0.5%nC_7H_{16}−22%O_2−77.5%He).

results showed that laminar burning velocities and flame instabilities of the mixtures were relatively sensitive to the *n*-heptane content less than 25%. Recently, Liang et al.[34] in our research group measured the ignition delay times of methane−*n*-heptane mixtures at different methane contents and various initial temperatures through a shock tube setup, and the comparisons between the experimental and numerical values of ignition delay times of the mixtures were done, through which the applicability of the reaction mechanisms in the simulation of the zero-dimensional constant-volume adiabatic ignition processes of the mixtures was validated. However, the species profiles of methane oxidation with *n*-heptane addition were rarely characterized, and the kinetic effects of *n*-heptane on the oxidation of methane was also not studied in detail.

Therefore, the objective of the present study is to investigate the low and high temperature mutual oxidation characteristics of the methane/*n*-heptane mixture. In the study, methane/*n*-heptane oxidation was investigated over a range of temperatures from 800 to 1200 K, at the equivalence ratio of 0.5 in an atmospheric jet-stirred reactor (JSR). The *n*-heptane contents in the methane/*n*-heptane mixture were varied between 0 and 100%. The mole fractions of CH_4, nC_7H_{16}, O_2, CO, CO_2, CH_2O, and C_2H_4 were determined respectively in the present experiments. Besides, the reaction path analysis of the methane/*n*-heptane mixture and the sensitivity analysis of the mole fraction of methane were performed under the relevant conditions to understand the kinetic enhancement of methane oxidation by *n*-heptane addition.

2. EXPERIMENTAL METHODS AND KINETIC MODELS

2.1. Experimental Setup. The oxidation of methane/*n*-heptane mixture was experimentally conducted in a JSR developed in Princeton University.[35−37] The reactor consists of a fused silica sphere with an internal volume of 42 cm^3, equipped with four nozzles of 1 mm diameter. High turbulence is created through the nozzles, achieving homogeneity in composition of the gas phase. It is located inside a stainless-steel jacket with a regulated electrical resistance heating system, and surrounded by insulating silica wool, allowing operation up to 1300 K.

During the process, mass-flow controllers (MKS, 0.5% uncertainty) were employed to regulate all the gases (CH_4, O_2, Ar, and N_2) flow rates, and a syringe pump (Harvard Apparatus, PHD 22/2000) was used to deliver liquid *n*-heptane to a prevaporizer. The methane and vaporized *n*-heptane gas were diluted by heated nitrogen for atomization, and preheated to reach the reaction temperature to minimize temperature gradients in the JSR. Then, this fuel-nitrogen flow was mixed with the O_2/Ar/N_2 flow just before the entrance of the injectors. The products were analyzed directly by microgas chromatography (μ-GC, Inficon 3000) through sonic probes sampling. It was used for the quantification of major combustion species (*n*-heptane, CH_4, O_2, CO, CO_2, CH_2O, and C_2H_4) within a 5% uncertainty, and detailed information about this facility was shown in refs 38−40.

DOI: 10.1021/acs.energyfuels.8b03124
Energy Fuels 2018, 32, 11970−11978

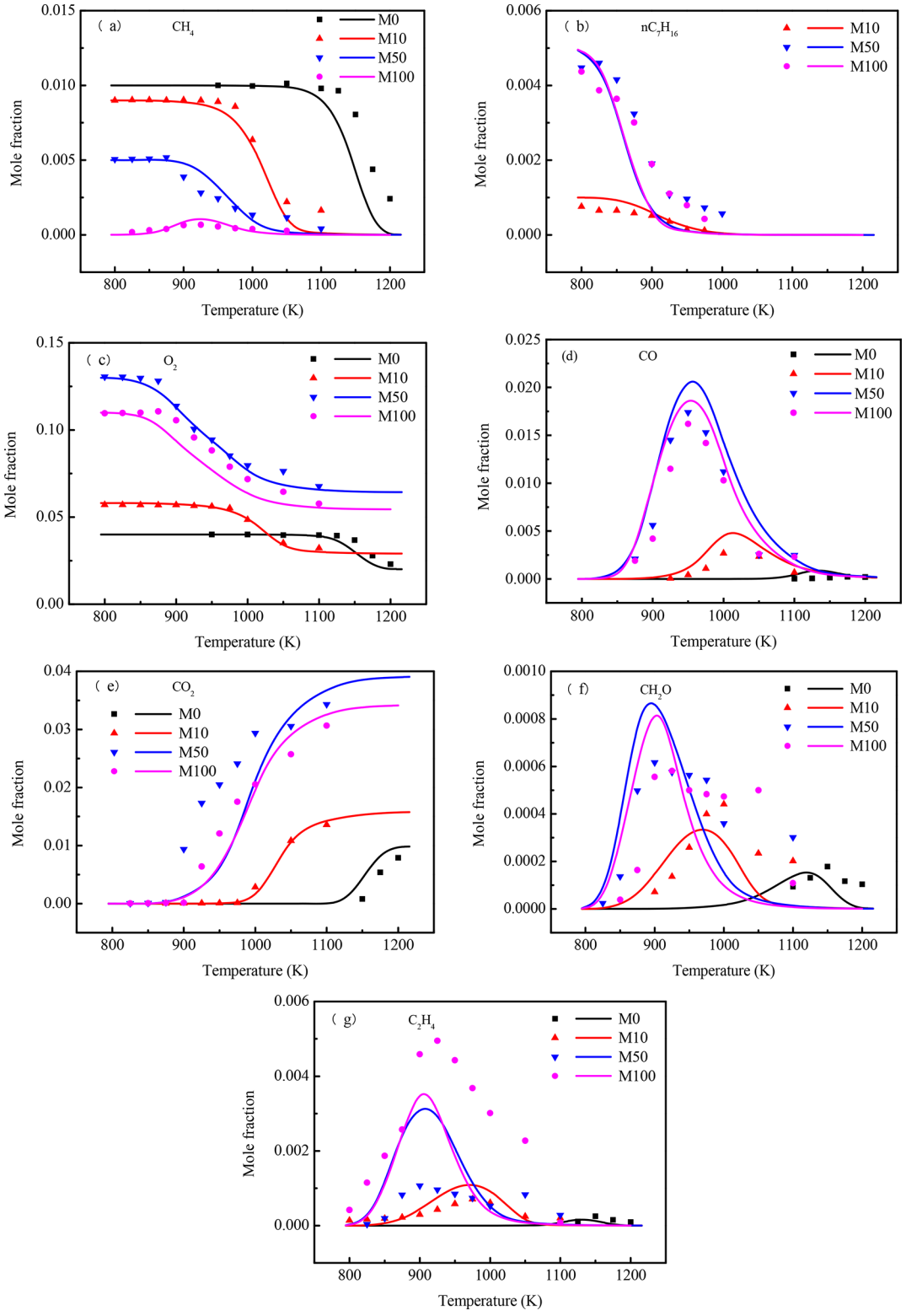

Figure 2. Variations of the mole fractions of important species with temperatures at different *n*-heptane contents (ϕ = 0.5, P = 1 atm).

The experiments were conducted under engine-like conditions at an equivalence ratio of 0.5, taking account of the fact that natural gas–diesel dual-fuel engines often operate under lean burned condition for the reduction of the nitrogen oxide emissions.[41,42] The temperatures range from 800 to 1200 K, which cover the low and high temperature regions of the oxidation of methane, while under 800 K, there is no methane oxidation. The initial pressure is 1 atm, and the gas flow rate is 1800 mL/min. As such, the residence time in the reactor varies with reactor temperature through the following equation.

$$\tau = (V/\upsilon)T_0/T \quad (1)$$

where V is the volume of the JSR, υ is the inlet volume flow rate at room temperature, T_0 is the room temperature (295 K).[43,44] The *n*-heptane content is defined as the mole fraction of *n*-heptane in the methane/*n*-heptane mixture at the initial experimental conditions, which covers a

DOI: 10.1021/acs.energyfuels.8b03124
Energy Fuels 2018, 32, 11970−11978

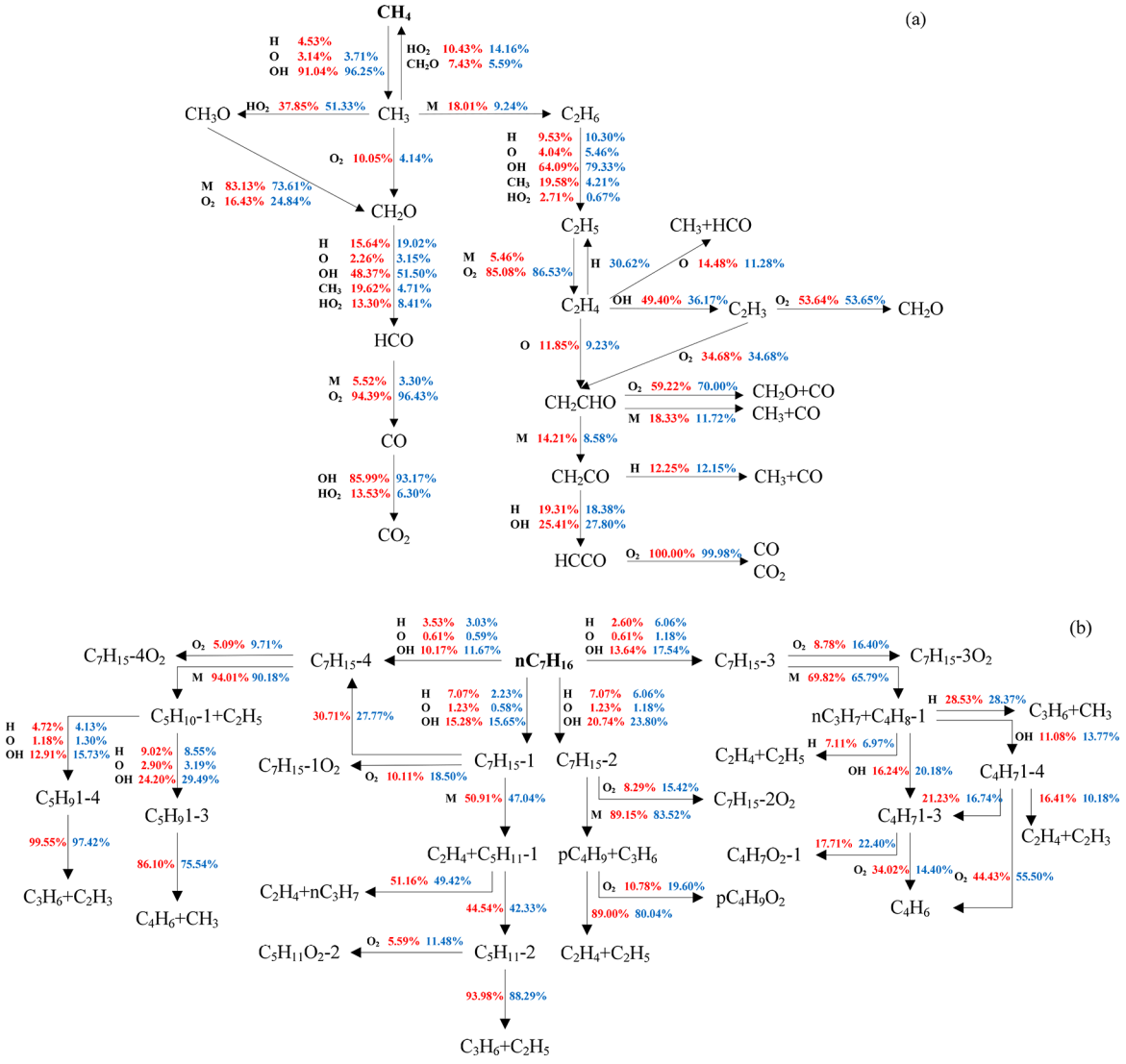

Figure 3. Reaction path analyses for methane and *n*-heptane in the mixture with 10% *n*-heptane (red) and 50% *n*-heptane (blue) addition at 950 K, 1 atm, and the equivalence ratio of 0.5.

range of 0−100%. For simplicity, M0 denotes pure methane at an *n*-heptane content of 0% by mole fraction and M100 denotes pure *n*-heptane in the present study, etc. The detailed experimental conditions are listed in Table 1.

2.2. Kinetic Mechanism. The detailed submechanism of methane is always included in the chemical kinetic mechanism of *n*-heptane,[26,45−50] as methane is one of the most important intermediate species in the combustion of *n*-heptane. Thus, a detailed chemical kinetic mechanism of *n*-heptane recently proposed by Zhang et al.,[45] consisting of 1268 species and 5336 elementary reactions, is adopted to carry on the present simulations and kinetic analysis, and denoted as the NUI mechanism in the paper.

To validate that the NUI mechanism can be used in the present study, experiments were performed to obtain the mole fractions of the major species during the oxidation of *n*-heptane at a pressure of 1 atm and the equivalence ratio of 0.5. All simulations were performed in the perfectly stirred reactor model[51] within CHEMKIN-PRO software[52] employing the transient solver, and the numerical results were compared with the experimental data from the present study and other data in the literature. The species concentration profiles are shown in Figure 1. It can be seen from Figure 1 that the NUI mechanism behaves well in the prediction of the mole fractions of CH_4, nC_7H_{16}, O_2, and CO_2 during the *n*-heptane oxidation process under the atmospheric and lean-burned conditions. In addition, it is also observed that the tendency of the experimental data of the present study is similar to that of Herbinet et al.[45] at the equivalence ratio of 0.25, indicating that the reliability of the experimental facility in this study is acceptable.

3. RESULTS AND DISCUSSION

3.1. Species Temperature Evolution. The mole fractions of CH_4, nC_7H_{16}, O_2, CO, CO_2, CH_2O and C_2H_4 during the oxidation of methane, *n*-heptane, and methane/*n*-heptane mixture were determined respectively by using the experimental facility mentioned above, and the results of the comparisons between the experimental values and numerical ones were displayed in Figure 2. As seen in Figure 2, this mechanism can in general predict the mole fractions of important species in the oxidation of the mixture at different *n*-heptane contents well. Since the C_0−C_4 submechanism of the NUI mechanism is obtained from the newly updated AramcoMech 2.0,[53] the simulation results of the species concentrations in the oxidation of pure methane are also in good agreement with the experimental data.

Figure 2a−e present the variations of the mole fractions of reactants (CH_4, nC_7H_{16}, and O_2) and product (CO and CO_2) with temperatures. From these plots, it is seen that the onset of

DOI: 10.1021/acs.energyfuels.8b03124
Energy Fuels 2018, 32, 11970−11978

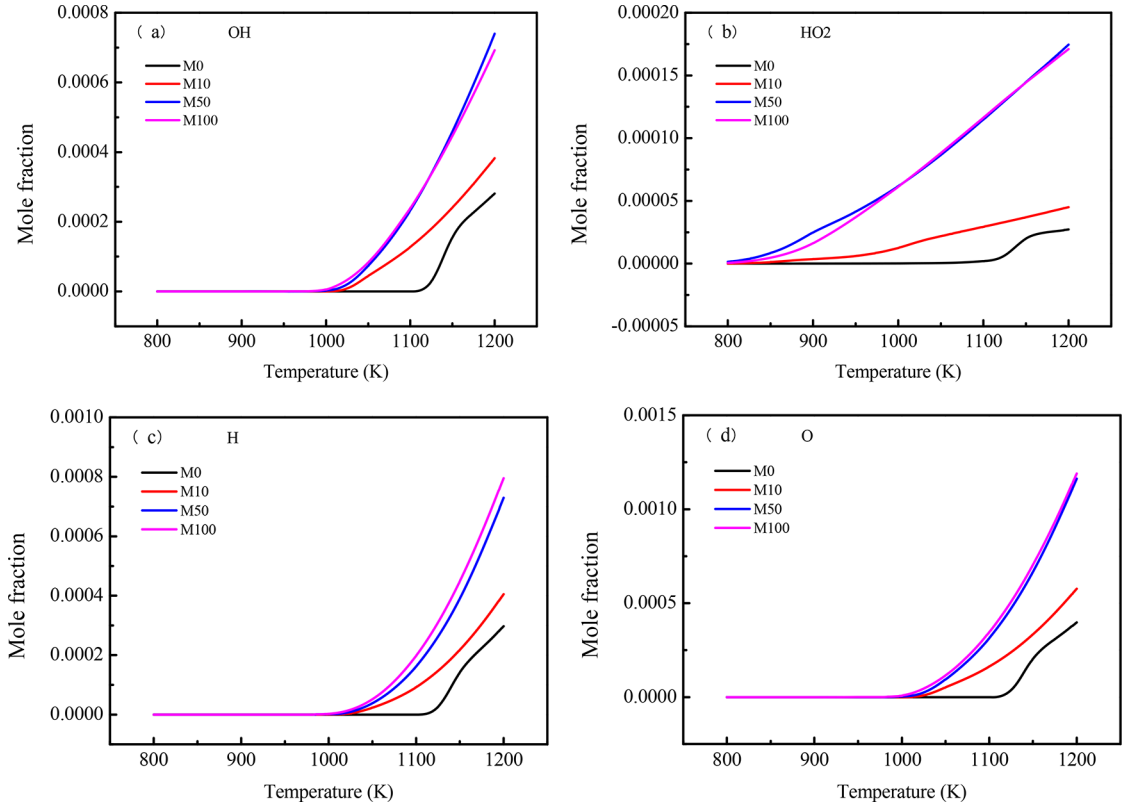

Figure 4. Variations of the simulated mole fractions of OH, HO_2, H, and O with temperatures at different *n*-heptane contents (ϕ = 0.5, P = 1 atm).

the oxidation of *n*-heptane is around 800 K, while the oxidation of methane starts at relatively higher temperatures under the conditions of present study. As seen in Figure 2, the oxidation of neat methane starts around 1050 K under fuel-lean conditions, with O_2 slightly consumed and a small amount of CH_2O detected at that moment. At higher temperatures, CO, CO_2, and C_2H_4 are also observed. Between 1100 and 1200 K, the mole fraction of methane decreases rapidly when the consumption of O_2 is accelerated, and the mole fractions of CH_2O and C_2H_4 reach the peaks. Methane is completely converted at about 1200 K, and the intermediates are transformed to the final product of CO_2. While the *n*-heptane contents are 10% and 50% in the methane/*n*-heptane mixture, the onset temperatures of methane reactions are about 900 and 850 K, respectively. This indicates that as the *n*-heptane content increases, the onset temperatures of the oxidation of methane decrease. Moreover, the results of the mole fraction profiles during the oxidation of the methane/*n*-heptane mixture reveal that the onset temperatures of methane oxidation vary nonlinearly with the *n*-heptane content. It is observed that a small amount of *n*-heptane in the methane/*n*-heptane mixture has a relatively significant promotion on the oxidation of methane, while more *n*-heptane addition has a marginal effect. In addition, it is seen that the major products are well predicted by the model at different fuel blends.

Figure 2 panels f and g give the variations of the mole fractions of major intermediates (CH_2O and C_2H_4) with temperature, which are considered as the important oxygenated species and unsaturated hydrocarbon, respectively, and are also critical references to the onset of the oxidation process. Although the species profiles are overpredicted at high *n*-heptane contents, the trends of the changes are reasonably predicted by the model, showing the need for further study and optimization of this mechanism. It is also notable that the generation of C_2H_4 is apparently larger, compared to that of CH_2O.

3.2. Reaction Path Analysis. To better understand the oxidation process of methane with *n*-heptane addition, the reaction path analyses for the mixture at the *n*-heptane contents of 10% and 50% were performed under the experimental conditions, respectively, as shown in Figure 3. According to the results, a relatively obvious discrepancy in the consumption pathways of methane at different *n*-heptane contents is observed, while the oxidation processes of *n*-heptane are almost in the same way.

For the methane/*n*-heptane mixture at *n*-heptane content of 10%, methane is mainly converted to CH_3 radicals through the H-abstraction at the beginning of the process, and the methane reaction with OH via R46 $CH_4 + OH \leftrightarrow CH_3 + H_2O$ has the most remarkable contribution to the methane consumption, accounting for 91.04%. There are four channels for the conversion of CH_3. At low temperature, most of CH_3 react with HO_2 to form CH_3O which is converted to CH_2O subsequently, and 10.05% CH_3 are oxidized by O_2 to form CH_2O directly through the reaction R91 $CH_3 + O_2 \leftrightarrow CH_2O + OH$. Then, the formed CH_2O entirely undergoes the H-abstraction with H, O, and OH radicals, and produces HCO which then is transformed into CO and CO_2 as the final products in the oxidation of methane. The rest of CH_3 mainly react with HO_2 and CH_2O to form CH_4, and with CH_3 to generate C_2H_6. When the *n*-heptane content increases to 50%, due to the increase of free radicals, it is found that the H abstraction of CH_4 by OH and CH_3 oxidation by HO_2 are enhanced to some extent. In addition, another recombination reaction occurs between C_2H_4 and the H atom.

In the oxidation of *n*-heptane, the fuel molecules entirely proceed the H-abstraction and yield four different isomers of

DOI: 10.1021/acs.energyfuels.8b03124
Energy Fuels 2018, 32, 11970−11978

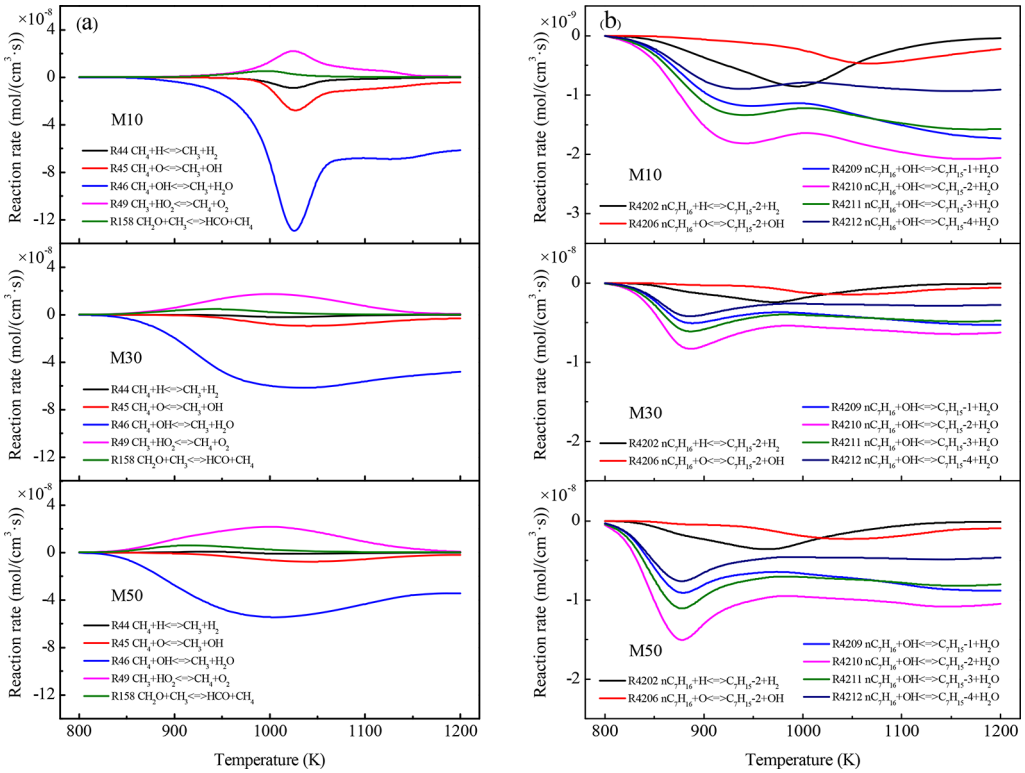

Figure 5. Profiles of the reaction rates of the initial promoting elementary reactions related to the fuel consumption and formation in the oxidation of the methane/*n*-heptane mixture at different *n*-heptane contents (ϕ = 0.5, P = 1 atm).

C_7H_{15}, mostly by OH radicals through the reaction nC_7H_{16} + OH ↔ C_7H_{15} + H_2O. Then the β-scission is the dominant decomposition path for the formed alkyl radicals C_7H_{15} in the low temperature oxidation of *n*-heptane. C_7H_{15} are converted into olefins and other alkyl radicals, which subsequently decompose into small molecule hydrocarbons, such as C_2H_4. This is the reason why the production of C_2H_4 is found to be apparently larger than that of CH_2O in Figure 2. Compared to the mixture at 10% *n*-heptane content, all the oxygen addition pathways are significantly promoted when the *n*-heptane content is 50%, and as a result, the efficient β-scission channels will be inhibited.

To further verify the analysis in Figure 2 and Figure 3, the mole fractions of the radical pool (OH, HO_2, H, and O) in simulations are also plotted in Figure 4 to clarify the oxidation reactivity among different fuel blends. It is seen that the mole fractions of OH, HO_2, H, and O increase significantly with *n*-heptane addition, especially at lower temperatures, while there is nearly no difference between M50 and M100. Therefore, it confirms that a small amount of *n*-heptane addition could accelerate the methane ignition dramatically through the radical pool enrichment. The promoting effect becomes insensitive to *n*-heptane addition once the radical pool is established.

As illustrated above, the onset of the oxidation of methane is decreasing with the elevating *n*-heptane content in the methane/*n*-heptane mixture. Besides, it is revealed that H-abstraction from CH_4 and CH_3 oxidation by HO_2 are both promoted with the increase of *n*-heptane content. Hence, the initial promoting reactions related to the fuel consumption and formation are picked up here, and the variations of the rates of those elementary reactions with temperatures are presented in Figure 5. It can be seen that the reaction rates of methane reactions begin to rise at about 900 K in the methane/*n*-heptane mixture with 10% *n*-heptane addition, which corresponds to the onset temperature of methane consumption in Figure 2. At 1000–1050 K, the reaction rates reach the peaks, which are also related to the accelerated oxidation process. When the *n*-heptane content increases, similarities are also obtained, and the nonlinear promoting effect of *n*-heptane addition on the onset of those reactions is found. Different from methane, all the H-abstractions of *n*-heptane are observed to start at 800 K. This is due to the weaker carbon–hydrogen bond in *n*-heptane than that in methane, and thus the oxidation reaction of *n*-heptane is observed to take place at the relatively lower temperature.

3.3. Sensitivity Analysis. The sensitivity analysis of the mole fractions of methane at different *n*-heptane contents is performed at 950 K, 1 atm, and the equivalence ratio of 0.5 to find out the most important reactions that influence the oxidation of methane, as shown in Figure 6. The sensitivity coefficient is defined as,

$$S = \frac{\partial \ln c_j}{\partial \ln k_i} \tag{2}$$

where c_j is the mole fraction and k_i is the specific rate coefficient. A positive sensitivity coefficient denotes that the reaction inhibits reactivity and vice versa. From this figure, it is seen that the reactions with positive sensitivity coefficients are those relevant reactions which consume OH, HO_2, and other free radicals, and causes a reduced reactivity, while the reactions with negative sensitivity coefficients are mainly the chain-branching reactions where OH and other reactive species are produced, then promoting the oxidation process.

In addition, Figure 7 gives the variations of the net reaction rates of those most important elementary reactions selected from Figure 7 with temperatures, and the same tendency is found with the results in Figure 5. That is, when the content of *n*-

DOI: 10.1021/acs.energyfuels.8b03124
Energy Fuels 2018, 32, 11970–11978

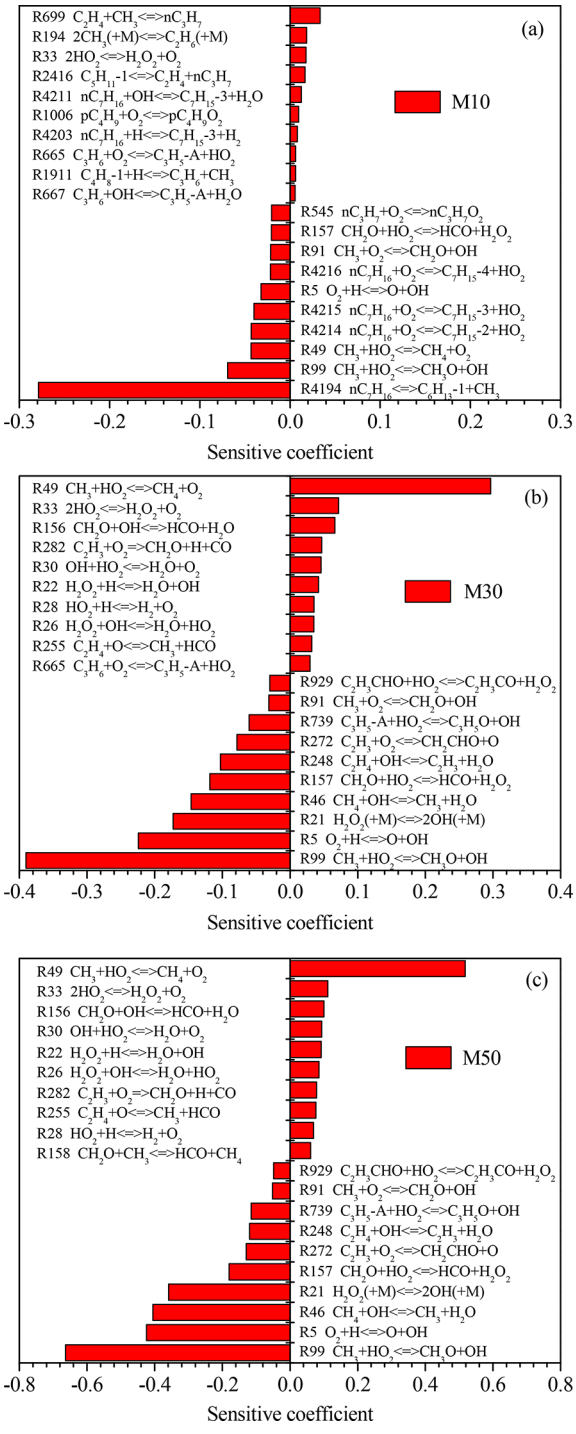

Figure 6. Sensitivity analysis of the mole fraction of methane at 950 K, 1 atm, and the equivalence ratio of 0.5.

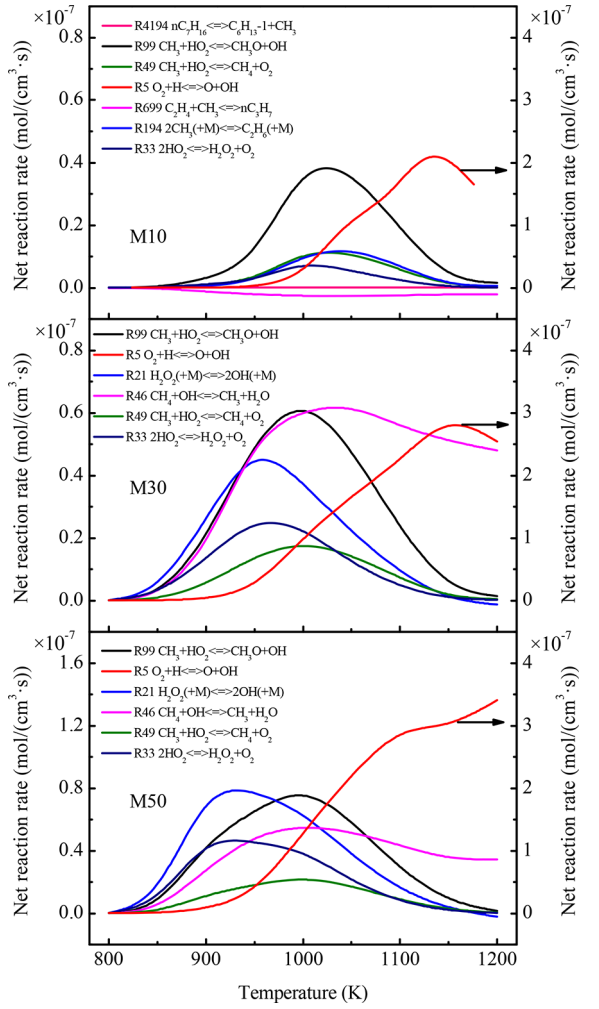

Figure 7. Profiles of the net reaction rates of the most important elementary reactions in the oxidation of the methane/*n*-heptane mixture at different *n*-heptane contents (ϕ = 0.5, P = 1 atm).

heptane is elevated, the onset temperatures of those most important elementary reactions are advanced, which leads to the early oxidation of methane. Here, regardless of the *n*-heptane content, the net reaction rates of the reactions that have negative sensitivity coefficients are greater than those of the reactions that have positive sensitivity coefficients, enabling the radical pool to increase gradually.

According to the sensitivity analysis of the mole fraction of methane and the results of the net reaction rates, the reaction R49 $CH_3 + HO_2 \leftrightarrow CH_4 + O_2$ is the most inhibiting reaction in the mixture at the *n*-heptane contents of 30% and 50%, through which CH_3 reacts with HO_2 to reform methane, so the oxidation process of methane is inhibited. Meanwhile, the reactions R99 $CH_3 + HO_2 \leftrightarrow CH_3O + OH$, R5 $O_2 + H \leftrightarrow O + OH$ and R21 H_2O_2 (+M) $\leftrightarrow$ 2OH (+M) are the significant promoting reactions that will yield OH, and thus enhance the overall reactivity. The reaction R46 $CH_4 + OH \leftrightarrow CH_3 + H_2O$ is also found to be considerably important. With this consuming reaction, the concentration of methane tends to decrease gradually.

When the content of *n*-heptane is 10%, the most sensitive elementary reactions are quite different from the above results. It is worth noting that under the conditions studied, the sensitive reactions are those related reactions which *n*-heptane directly participates in, highlighting the importance of *n*-heptane controlling chemistry in the oxidation of methane at high temperatures. The reactions R4211 $nC_7H_{16} + OH \leftrightarrow C_7H_{15}$-3 + H_2O and R4203 $nC_7H_{16} + H \leftrightarrow C_7H_{15}$-3 + H_2 are the important inhibiting reactions, through which OH and H in the radical pool are consumed, and overall reactivity is reduced. The chain branching reactions R4194 $nC_7H_{16} \leftrightarrow C_6H_{13}$-1 + CH_3, R4214 $nC_7H_{16} + O_2 \leftrightarrow C_7H_{15}$-2 + HO_2, R4215 $nC_7H_{16} + O_2 \leftrightarrow C_7H_{15}$-3 + HO_2 and R4216 $nC_7H_{16} + O_2 \leftrightarrow C_7H_{15}$-4 + HO_2 show the obvious positive effect on the oxidation of methane, resulting in the increased generation of free radicals and finally promoting

DOI: 10.1021/acs.energyfuels.8b03124
Energy Fuels 2018, 32, 11970−11978

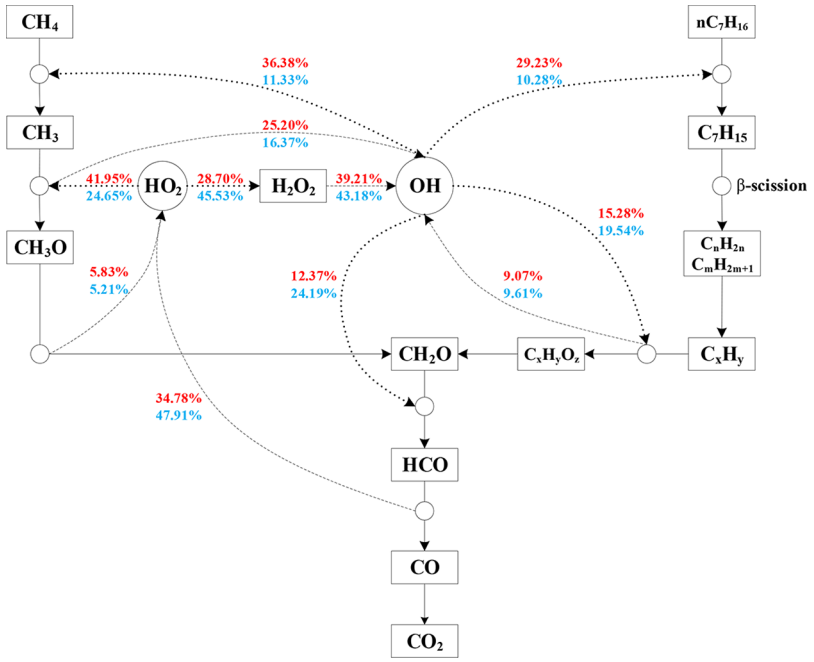

Figure 8. Oxidation pathways for the methane/*n*-heptane mixture with 10% *n*-heptane (red) and 50% *n*-heptane (blue) addition at 950 K, 1 atm, and the equivalence ratio of 0.5.

the oxidation process. It reveals that even a small amount of *n*-heptane addition could accelerate the methane ignition dramatically through the radical pool enrichment, such as OH and HO_2. The promoting effect becomes insensitive to *n*-heptane addition once the radical pool is established.

Since the free radicals such as OH and HO_2 play the important role in the kinetic reactions between methane and *n*-heptane, Figure 8 gives the main oxidation pathways for the methane/*n*-heptane mixture and the conversion ratios of those important radicals. In Figure 8, the solid lines represent the reaction process of major species, and the dash lines denote the production channels of radicals, while the dot lines indicate the consumption channels of radicals. The percentages are considered as the production and consumption values associated with OH and HO_2 radicals. According to the results, it is well recognized that *n*-heptane interacts with methane through the radical pool where OH and HO_2 are the most important radicals in the oxidation of the methane/*n*-heptane mixture. Because of the low carbon−hydrogen bond energy in *n*-heptane, the oxidation of *n*-heptane is assumed to start at lower temperatures, which will contribute to the remarkable production of free radicals, and then advance the oxidation of methane.

4. CONCLUSIONS

The kinetic effects of *n*-heptane addition on the oxidation of methane at 800−1200 K, 1 atm, and the equivalence ratio of 0.5 were experimentally and numerically investigated with the *n*-heptane content ranging from 0 to 100%. The main conclusions of the present study are summarized as follows:

1. As the content of *n*-heptane in the methane/*n*-heptane mixture increases, the onset temperature of the oxidation of methane decreases and a nonlinear relationship between the onset temperature and the *n*-heptane content is observed. That is, a small amount of *n*-heptane has a relatively significant promotion on the oxidation of methane, while the addition of more *n*-heptane has less kinetic enhancement effect.
2. The reaction path analysis of the methane/*n*-heptane mixture indicates that the oxidation process of methane is changed by the addition of *n*-heptane. With the increase of *n*-heptane content, the H abstraction of CH_4 by OH and CH_3 oxidation by HO_2 are enhanced. Then, the initial kinetic enhancement reactions of methane oxidation by *n*-heptane addition are identified, and the reaction rates of those reactions are observed to begin to rise at lower temperatures.
3. According to the results of the sensitivity analysis and the net reaction rates of the most important elementary reactions, the mole fraction of methane is more sensitive to the reactions related to OH and HO_2 radicals, and the addition of *n*-heptane is found to contribute to the early formation of free radicals. In addition, it is seen that when the *n*-heptane content is 10%, reactions involving in *n*-heptane promote the methane oxidation significantly, while the promoting effect becomes insensitive when *n*-heptane content rises from 10% to 50%. This reveals that even a small amount of *n*-heptane addition could accelerate the methane ignition dramatically through the radical pool enrichment, such as HO_2 and OH. The promoting effect becomes insensitive to *n*-heptane addition once the radical pool is established.

Therefore, the present study indicates the potential of *n*-heptane-assisted methane combustion in diesel and marine engine applications.

AUTHOR INFORMATION

Corresponding Author

*E-mail: haozhao@princeton.edu.

ORCID

Zunhua Zhang: 0000-0003-4445-180X

Hao Zhao: 0000-0002-8879-9595

DOI: 10.1021/acs.energyfuels.8b03124
Energy Fuels 2018, 32, 11970−11978

Author Contributions

[#]Z.Z. and H.Z. contributed equally to the work.

Notes

The authors declare no competing financial interest.

■ ACKNOWLEDGMENTS

This work is partly supported by the Natural Science Foundation of China (Grants 51479149 and 51779199), NSF CBET-1507358 research grant, and the Princeton Environmental Institute (PEI)-Andlinger Center for Innovative Research Awards in Energy and the Environment.

■ REFERENCES

(1) Cho, H. M.; He, B. Q. *Energy Convers. Manage.* **2007**, *48*, 608−618.
(2) Papagiannakis, R. G.; Hountalas, D. T. *Energy Convers. Manage.* **2004**, *45*, 2971−2987.
(3) Aslam, M. U.; Masjuki, H. H.; Kalam, M. A.; Abdesselam, H.; Mahlia, T. M. I.; Amalina, M. *Fuel* **2006**, *85*, 717−724.
(4) Kalam, M. A.; Masjuki, H. H. *Energy* **2011**, *36*, 3563−3571.
(5) Carlucci, A. P.; Risi, A. D.; Laforgia, D.; Naccarato, F. *Energy* **2008**, *33*, 256−263.
(6) Cordiner, S.; Gambino, M.; Iannaccone, S.; Rocco, V.; Scarcelli, R. *Energy Fuels* **2008**, *22*, 1418−1424.
(7) Mansour, C.; Bounif, A.; Aris, A.; Gaillard, F. *Int. J. Therm. Sci.* **2001**, *40*, 409−424.
(8) Wei, L.; Geng, P. *Fuel Process. Technol.* **2016**, *142*, 264−278.
(9) Zhang, Q.; Li, M.; Shao, S. *Appl. Energy* **2015**, *157*, 217−228.
(10) Liu, J.; Yang, F.; Wang, H.; Ouyang, M.; Hao, S. *Appl. Energy* **2013**, *110*, 201−206.
(11) Papagiannakis, R. G.; Rakopoulos, C. D.; Hountalas, D. T.; Rakopoulos, D. C. *Fuel* **2010**, *89*, 1397−1406.
(12) Papagiannakis, R. G.; Hountalas, D. T. *Appl. Therm. Eng.* **2003**, *23*, 353−365.
(13) Westbrook, C. K.; Pitz, W. J.; Mehl, M.; Curran, H. J. *Proc. Combust. Inst.* **2011**, *33*, 185−192.
(14) Mehl, M.; Pitz, W. J.; Westbrook, C. K.; Curran, H. J. *Proc. Combust. Inst.* **2011**, *33*, 193−200.
(15) Mueller, C. J.; Cannella, W. J.; Bruno, T. J.; Bunting, B.; Dettman, H. D.; Franz, J. A.; et al. *Energy Fuels* **2012**, *26*, 3284−3303.
(16) Ranzi, E.; Frassoldati, A.; Stagni, A.; Pelucchi, M.; Cuoci, A.; Faravelli, T. *Int. J. Chem. Kinet.* **2014**, *46*, 512−542.
(17) Hu, E.; Huang, Z.; He, J.; Miao, H. *Int. J. Hydrogen Energy* **2009**, *34*, 6951−6960.
(18) Ying, Y.; Liu, D. *Int. J. Hydrogen Energy* **2015**, *40*, 3777−3788.
(19) Zhao, W.; Yang, W.; Fan, L.; Zhou, D.; Ma, X. *Appl. Therm. Eng.* **2017**, *123*, 1060−1071.
(20) Hockett, A.; Hampson, G.; Marchese, A. J. *Energy Fuels* **2016**, *30* (3), 2414.
(21) Luo, M.; Liu, D. *Int. J. Hydrogen Energy* **2016**, *41*, 11471−11480.
(22) Jia, P.; Ying, Y.; Luo, M.; Jiang, B.; Liu, D. *Appl. Therm. Eng.* **2018**, *139*, 11−24.
(23) Tang, C.; Wei, L.; Zhang, J.; Man, X.; Huang, Z. *Energy Fuels* **2012**, *26*, 6720−6728.
(24) Chen, Z.; Qin, X.; Ju, Y.; Zhao, Z.; Chaos, M.; Dryer, F. L. *Proc. Combust. Inst.* **2007**, *31*, 1215−1222.
(25) Burke, U.; Somers, K. P.; O'Toole, P.; Zinner, C. M.; Marquet, N.; Bourque, G.; et al. *Combust. Flame* **2015**, *162*, 315−330.
(26) Curran, H. J.; Gaffuri, P.; Pitz, W. J.; Westbrook, C. K. *Combust. Flame* **1998**, *114*, 149−177.
(27) Dagaut, P.; Reuillon, M.; Cathonnet, M. *Combust. Flame* **1995**, *101*, 132−140.
(28) Dames, E. E.; Rosen, A. S.; Weber, B. W.; Gao, C. W.; Sung, C. J.; Green, W. H.; et al. *Combust. Flame* **2016**, *168*, 310−330.
(29) Jiang, X.; Tian, Z.; Zhang, Y.; Huang, Z. *Fuel* **2017**, *203*, 316−329.
(30) Reuter, C. B.; Zhang, R.; Yehia, O. R.; Rezgui, Y.; Ju, Y. *Combust. Flame* **2018**, *196*, 1−10.
(31) Aggarwal, S. K.; Awomolo, O.; Akber, K. *Int. J. Hydrogen Energy* **2011**, *36*, 15392−15402.
(32) Wang, Z.; Abraham, J. *Proc. Combust. Inst.* **2015**, *35*, 1041−1048.
(33) Li, G.; Liang, J.; Zhang, Z.; Tian, L.; Cai, Y.; Tian, L. *Energy Fuels* **2015**, *29*, 4549−4556.
(34) Liang, J.; Zhang, Z.; Li, G.; Wan, Q.; Xu, L.; Fan, S. *Fuel* **2019**, *235*, 522−529.
(35) Zhao, H.; Wu, L.; Patrick, C.; Zhang, Z.; Rezgui, Y.; Yang, X.; et al. *Combust. Flame* **2018**, *197*, 78−87.
(36) Zhang, T.; Zhao, H.; Ju, Y. *AIAA J.* **2018**, *56*, 1−5.
(37) Zhao, H.; Dana, A.; Zhang, Z.; Green, W.; Ju, Y. *Energy* **2018**, *165*, 727−738.
(38) Zhao, H.; Fu, J.; Haas, F. M.; Ju, Y. *Combust. Flame* **2017**, *183*, 253−260.
(39) Zhao, H.; Fu, J.; Ju, Y. *In: 55th AIAA Aerospace Sciences Meeting* **2017**, 1964.
(40) Tran, L. S.; Pieper, J.; Carstensen, H. H.; Zhao, H.; Isabelle, G.; Ju, Y.; Graf, I.; Kohse-Hoinghaus, K.; et al. *Proc. Combust. Inst.* **2017**, *36*, 1165−1173.
(41) Adachi, S.; Iwamoto, A.; Hayashi, S.; Yamada, H.; Kaneko, S. *Proc. Combust. Inst.* **2007**, *31*, 3131−3138.
(42) Ibrahim, A.; Bari, S. *Energy Convers. Manage.* **2009**, *50*, 3129−3139.
(43) Zhao, H.; Yang, X.; Ju, Y. *Combust. Flame* **2016**, *173*, 187−194.
(44) Felsmann, D.; Zhao, H.; Wang, Q.; Graf, I.; et al. *Proc. Combust. Inst.* **2017**, *36*, 543−551.
(45) Zhang, K.; Banyon, C.; Bugler, J.; Curran, H. J.; Rodriguez, A.; Herbinet, O.; et al. *Combust. Flame* **2016**, *172*, 116−135.
(46) Lu, T.; Law, C. K. *Combust. Flame* **2008**, *154*, 153−163.
(47) Lu, T.; Law, C. K. *Combust. Flame* **2006**, *144*, 24−36.
(48) Herbinet, O.; Husson, B.; Serinyel, Z.; Cord, M.; Warth, V.; Fournet, R.; et al. *Combust. Flame* **2012**, *159*, 3455−3471.
(49) Prince, J. C.; Williams, F. A.; Ovando, G. E. *Fuel* **2015**, *149*, 138−142.
(50) Hakka, H. M.; Cracknell, R. F.; Pekalski, A.; Glaude, P. G.; Battin-Leclerc, F. *Fuel* **2015**, *144*, 358−368.
(51) Glarborg, P.; Kee, R. J.; Grcar, J. F.; Miller, J. A. *PSR: A Fortran program for modeling well-stirred reactors*; Sandia National Labs: Livermore, CA, 1986; Report SAND86-8209.
(52) Kee, R. J.; Rupley, F. M.; Miller, J. A.; *Chemkin-II: A Fortran chemical kinetics package for the analysis of gas-phase chemical kinetics*; Sandia National Labs: Livermore, CA, 1989; Report SAND89-8009.
(53) Metcalfe, W. K.; Burke, S. M.; Ahmed, S. S.; Curran, H. J. *Int. J. Chem. Kinet.* **2013**, *45*, 638−675.

DOI: 10.1021/acs.energyfuels.8b03124
Energy Fuels 2018, 32, 11970−11978